Damage process in glass fiber reinforced polymer specimens using acoustic emission technique with low frequency acquisition

Composite Structures

Damage Process in Glass Fiber Reinforced Polymer Specimens Using Acoustic Emission Technique with Low Frequency Acquisition

Leandro Friedrich[1], Angélica Colpo[2], Anna Maggi[2], Tiago Becker[2], Giuseppe Lacidogna[3] and Ignacio Iturrioz[2]

[1]Department of Mechanical Engineering, Universidade Federal do Pampa, Av. Tiaraju 810, CEP 97546-550, Alegrete, Brazil.

[2]Mechanical Post-Graduate Program, Universidade Federal do Rio Grande do Sul, Sarmento Leite 425, CEP 90050-170, Porto Alegre, Brazil.

[3]Department of Structural, Geotechnical and Building Engineering, Politecnico di Torino, 24, Corso Duca degli Abruzzi, 10129 Torino, Italy.

Corresponding author: leandroffriedrich@gmail.com

ABSTRACT

The damage process in fiber-reinforced polymers (FRP) has been the subject of continuous studies in recent decades using different approaches. In particular, the acoustic emission technique has been proved to be a powerful tool in the monitoring of structures of this type of material due to the large acoustic activity

captured when this material is loaded to rupture. The present work explores several indexes that were calculated from the experimental recording of acoustic emission signals, and their efficiency in describing the failure process in structures. One of this index is originally proposed, the called c value and its sensibility it is compared with other classical parameters that are usually employed in the Acoustical Emission analysis. A 3-point bending test has been performed on a glass fiber reinforced polymer plate. Our own methodology was proposed to identify AE signals in semi-automatic manner. This methodology also allowed a faster analysis of the global parameters during the process data of the AE test. The global parameter evolution obtained from the acoustic emission data during the damage process could be considered as precursors of the more meaningful event and as an aid to understand in which way the structure is going to the collapse.

KEYWORDS: Acoustic emission parameters, Glass fiber reinforced polymer, Damage monitoring

NOMENCLATURE

N	cumulative number of events
A	signal amplitude
ζ, β	adjustment constants
b	*b*-value parameter
m	signal amplitude in logarithmic scale
m_c	magnitude of completeness
D	fractal dimension
F	frequency
E_e	event energy

α	cumulative number of events
f	characteristic frequency of the acoustic emission signals
γ	angular coefficient of log E_e x log f
c	c-value parameter
K	material stiffness
I	moment of inertia
ρ	mass density
E	Young's modulus
L	plate length
w_n	natural frequency

1. INTRODUCTION

The constant monitoring of structures is a necessary procedure since early fault detection enables the use of simpler and more economical methods for evaluation and repair. Quantitative analysis of damage in quasi-brittle materials where the development of micro cracking process govern the damage process can produce an abrupt collapse, and the distribution of micro cracks can become more dense, producing localization that results in a macro-fissure formation and subsequent unstable propagation. This monitoring, called as failure prediction, has a great interest for the aerospace, civil, and mechanical industries as it provides considerable gains in economic and safety aspects.

A promising nondestructive method for monitoring the damage process is the Acoustic Emission Technique (AET). This method can be performed under service conditions, only by imposing an increase in force or pressure, without causing the complete structure failure **[1]**. Acoustic Emission (AE) is a phenomenon caused by structural change in a solid, in which transient elastic waves are produced due to an abrupt internal change of the structure under study (rupture, dislocation, among other causes). AE waves, whose frequency varies from a few kHz to MHz, propagate in the material to the surface of the structure where they are detected by sensors that convert the deformation energy into electrical signals **[2-5]**.

In structures built with fiber-reinforced polymer to use the AET is especially useful. Experimental evidence has shown that in these cases, there is much important information in AE signals, and it is possible to distinguish the different failure modes that occur during the structure loaded. There is an expressive number of articles that illustrate this application, for example in Barile et al. **[6]** where a laminated Carbon Fiber Reinforced Plastics (CFRP) plate before and after suffering an impact load is analyzed using the AET to measure its residual strength. Different global AE parameters are correlated with the kind and level of damage in the post-impacted plate.

Djabali et al. **[7]** using AET and the Digital Image Correlation (DIC) studied the mechanical and damage behavior of a thick laminated carbon/epoxy composite through static and fatigue three-point bending tests. Three different types of AE signals recorded were associated with three damage modes: matrix cracking, delamination, and fiber breaking. In both types of tests, the parameters analyzed (amplitude, number of counts, duration, and cumulative AE energy) provided rather quantitative information about material damage. In Verbruggen et al. **[8]** a similar approach is used in order to monitor concrete beams externally reinforced with CFRP.

Ghaib et al. **[9]** studied the behavior of long and reinforced fiber polymer bars in the tensile test by analyzing parameters calculated from the information of the acoustic emission test

performed. In the case previously mentioned, for each signal the magnitude and frequency features during the damage process was determined. Different failure mechanisms were recorded as delamination, matrix cracking, fiber debonding, and fiber fracture in the evaluation of the relation between fiber inclination and composite failure modes.

Ramirez-Jimenez et al. **[10]** analyzed the AE signals in the frequency domain, correlating the results with different micro failure mechanisms such as fiber pullout, fiber/matrix slippage, and fiber breaking. Huguet et al. **[11]** use the acoustic emission signal parameters to identify and characterize the various damage mechanisms in stressed glass fiber reinforced polymer composite. The authors identified two modes of precursor failure: matrix fracture and fiber-matrix decohesion. With the aim of characterizing each mode, parameters such as number of events, signal duration, and average frequency were used. References **[12-17]** can also be cited to illustrate which parameters calculated from acoustic emission tests allow to study the evolution of damage in composite materials.

In the present work, the acoustic emission technique is applied in the damage evolution of a glass fiber-reinforced polymer composite (GFRP) plate during a bending test. With the aim to analyze the damage process, time, and frequency domain parameters were computed during the test. In addition, an original

methodology for determining the parameters that characterize each signal implemented in MATLAB software is presented.

2. THE ACOUSTIC EMISSION TECHNIQUE

The AE technique measures the stress waves produced by some abrupt change which could be, for example, the initiation and growth of micro-cracks. The AE signals also called "hits" are recorded by transducers mounted on the structure. As it is pointed out in Othsu et al. **[18]** there are differences between AE signals and AE events. The signals, are recorded independently by each sensor regardless of the source. An "Event" is identified by means of a group of signals (hits), all of them originating from the same sources. A typical AE detection system is shown in **Figure 1**. The changes in the internal sources produce elastic waves that propagate throughout the structure tested until the sensors attached at different places on the structure surface. Analysis of the events can provide useful information about the magnitude and location of the type of damage in structures **[19]**. Among the extensive existing bibliography, many books and papers about the topic can be cited, among them **[2, 20-22]**.

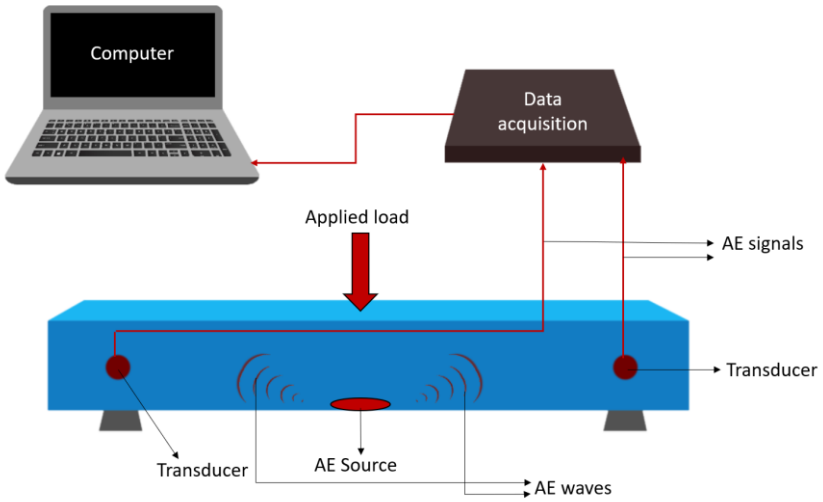

Figure 1. Schematic diagram of test specimen loading and AE test setup.

In **Figure 2** a typical signal of acoustic emission is presented with its main characteristic parameters. Among other parameters, there are the Maximum Amplitude and Duration of the signal which are both a function of the fixed Threshold Level. The Rise Time determines the time from the beginning of the signal until it reaches its maximum amplitude. The area under the signal function that is linked with the Energy dissipated in the damage process is also a significant parameter in the AE interpretation. Finally, the Frequency Content of the signals and its evolution during the AE test provide useful information on the damage process analyzed.

The study of the evolution of AE primary parameters extracted from the signals and their combination allows to find out more information about the damage process.

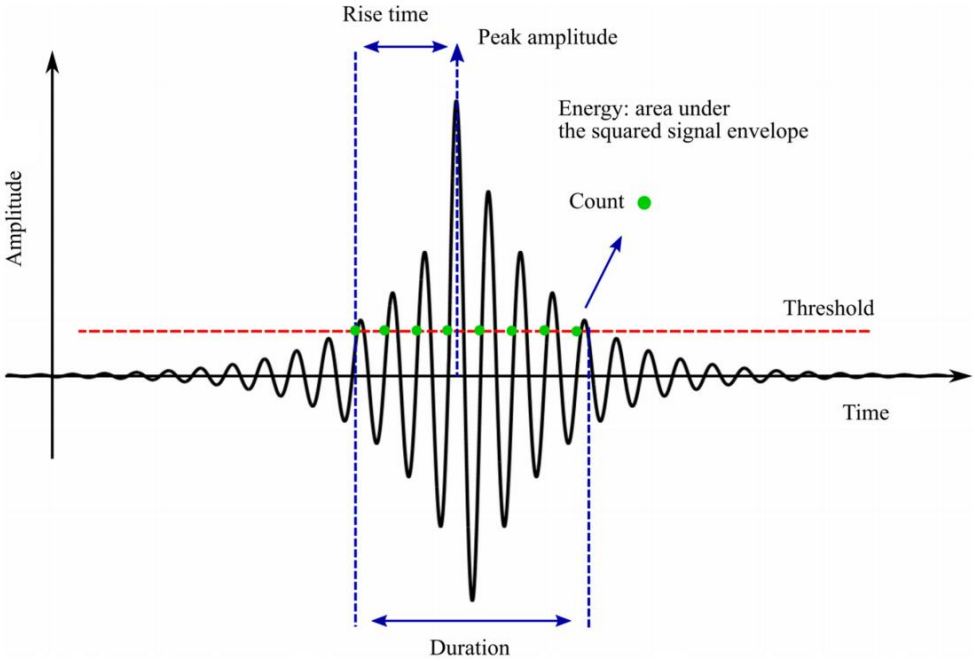

Figure 2. Common acoustic emission signal features (adapted from ref. **[23]**).

Next, we explain and describe in detail the characteristic of global parameters that were computed using the primary ones mentioned before:

(a) RA and AF relation: As previously pointed out by several researchers **[24-28]**, these parameters allow us to characterize the shape of the recorded emission wave, which is related to the failure mechanisms that produce it. The two parameters are the

rise angle (RA), that is, the ratio between the rise time (defined in **Figure 2)**, and the maximum amplitude of signal. On the other hand, the average frequency (AF) is defined as the number of counts divided by the duration of the signal. The definition of these parameters is also illustrated in **Figure 3a**.

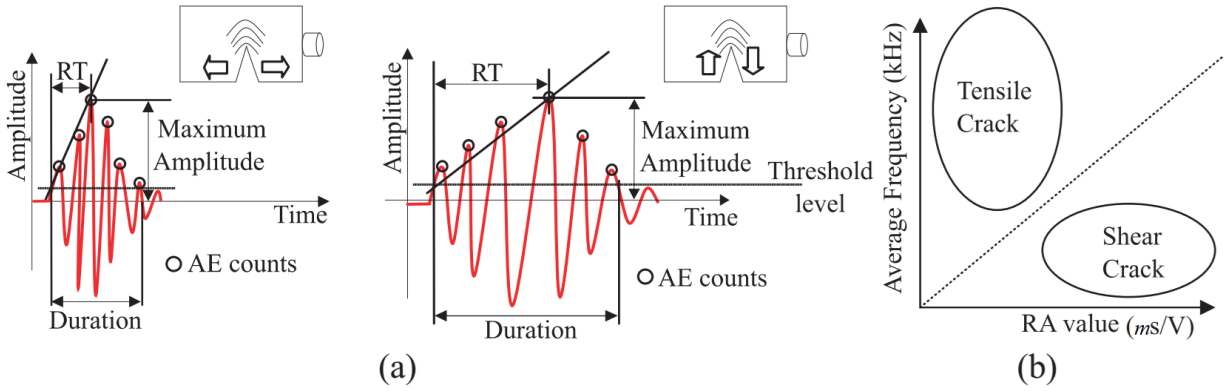

Figure 3. (a) Typical waveforms for tensile and shear signal (adapted from ref. **[26]**), (b) Relationship between average frequency and RA value (adapted from ref. **[29]**).

In those types of materials such as concrete, the relation between the RA and AF can be used to classify the type of failure in structures, as it is shown in **Figure 3b**. The signal is classified as shear mode (Mode II) when it has a low AF and a high RA value. In addition, the same signal is also classified as tensile mode (Mode I) when it has a high AF and low RA value as it is mentioned in **[26]** and **[30]**. An appropriate ratio between the abscissa and the ordinate should be chosen depending on the

material and the structure examined to determine the separation between Mode I and Mode II cracks.

This behavior was also noted in the study conducted by Soulioti et al. **[24]**, who analyzed the RA and AF parameters in EA signals on concrete materials containing different percentages of steel fiber under four-point testing. In this study, the authors cited here concluded that: Mode I and II are influenced by the increase in the addition of fibers. This has resulted in increased RA and decreased AF.

In this context, it could be noticed that in composite structures, the characterization of the signal using the RA x AF parameters is not directly associated with the fracture modes I and II. For example, the categorization using RA/AF ratio in composite laminates could be associated with the ability to identify the transition from matrix breakage to delamination **[31, 32]** or other characteristic failure mechanism, such as it was reported by Ghaib et al. **[9]**.

In De Sutter et al. **[19]** it is emphasized that the RA e AF parameters are to be crucial, particularly, in the composite where the fracture process is not directly linked to the temporal distribution of the AE signals.

(b) Evolution of *b*-value: Studies of seismology and its link to acoustic emission applications in engineering structures (with sizes in the order of meters) have remarkably enriched the theoretical framework in order to be able to link the AE and the

damage process in engineering structures. An illustrative example of this relation is the classic law proposed by Gutenberg & Ritcher **[33]**. This law relates the statistic of signal amplitudes using a universal exponential law. In accordance with Shiotani et al. **[2],** Hemmer and Hansen **[34]** and Hansen et al. **[35]** this is a Universal Law which does not depend on the scale of the distribution. This law could be expressed as follows:

$$N(\geq A) = \zeta A^{-b} \qquad \textbf{(1)}$$

where N is the cumulative number of events, A the signal amplitude and ζ and b are two adjustment constants. Defining $m = logA$ as another measure of the signal magnitude, we can rewrite Eq. (1) in the bi logarithmic domain as follows:

$$logN = log\zeta - bm \qquad \textbf{(2)}$$

where b will be the slope of the line that links the signals amplitude and the cumulative number of events, considering both variables on a logarithmic scale.

Aki **[36]** and Carpinteri et al. **[37, 38],** among others, discuss the physical meaning of the *b*-value, proposing that it could be related to the fractal dimension (D) of the domain from which the cracks emanate through the expression $D = 2b$. At the

beginning of the damage process in the structure, the events emanate from micro fissure distributed in a three dimensional (D) dimension i.e. (b = 1.5;(D=3), which can be interpreted, in terms of Eq. (2), as having more events that produce a small signal amplitude. The evolution of the damage process produces the localization effect, where events emanate from a preferential region in the form of a "cloud" made of micro fissures, resulting in the macro crack nucleation. In this last phase, the region where the acoustic events occur tends to have a surface dimension, i. e., D = 2 which implies that (b = 1.0). In the context of expression (2), this can be interpreted as the increment of events that produce larger signal amplitudes. **Figure 4** illustrates how the *b*-value typically varies during the process of the damage. Observing how the *b*-value changes during the damage process allows us to detect when and how the location of signals begins to appear in the analyzed structure.

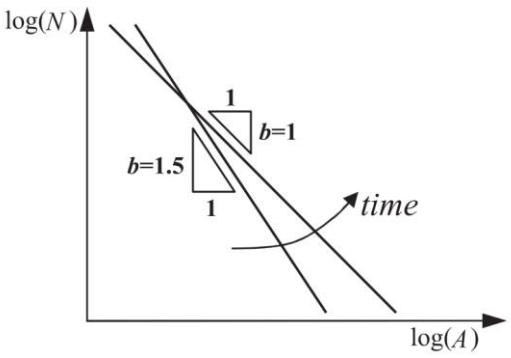

Figure 4. The *b*-value evolution in experimental test **[38].**

This effect often allows the prediction of a catastrophic failure to emerge. A deep discussion about how to compute the *b*-value could be found in Han et al. **[39].**

(c) Frequency fluctuations during the damage process: The dependence of the spectral density of frequency (SDF) is one of the essential characteristics of a fluctuational process **[40].** Furthermore, it can be observed that in many applications (as in geological, bioengineering, physiological and musical phenomena **[41]**) an increase in the magnitude of the spectral density of fluctuations when the frequency f decreases following an exponential variation **(**$SDF \sim f^{\gamma}$**).** Moreover, it was perceived that the tendency of the SDF function is inverted for low frequencies. The fluctuation that changes in this way is usually called "$1/f$ noise" or "flicker noise" **[40].** In various fields of science, the frequency statistics that characterize a signal have been studied, as it can be found in Gilden **[42]** and Milotti **[43].** When applying this idea to the context of acoustic emission, it would be possible to write that:

$$E_e = \alpha f^{\gamma} \tag{3}$$

where E_e represents the energy associated to the event and its frequency content is proportional to the Spectral Density function of the fluctuation registered by the AE device **[29].** In the

expression (3), f represents the frequency that characterizes the acoustic emission and α and γ scalar coefficients. By applying the logarithm in both terms in Equation (3) it results in:

$$logE_e = \log\alpha - \gamma \log f \quad \textbf{(4)}$$

where γ is the angular coefficient of the line that links the representative frequency interval in the signal. The index γ has been shown as an indicator of the change in the damage process pointing to the imminent collapse. Recently, Lacidogna et al. **[44]** used the evolution of γ in the evaluation of frequency distribution in laboratory concrete compression tests and in situ analysis of historic Italian constructions.

Figure 5 shows three typical signals characterized by the statistical distribution of their frequencies that appear in the most varied fields of science. The case of "white noise" that has a constant energy spectrum ($\gamma \approx 0$) reflecting the lack of correlation between the fluctuations. There is also a "pink noise" and a "brown noise", which indicates that the structure has a preference to a dissipate energy correlated with certain frequencies.

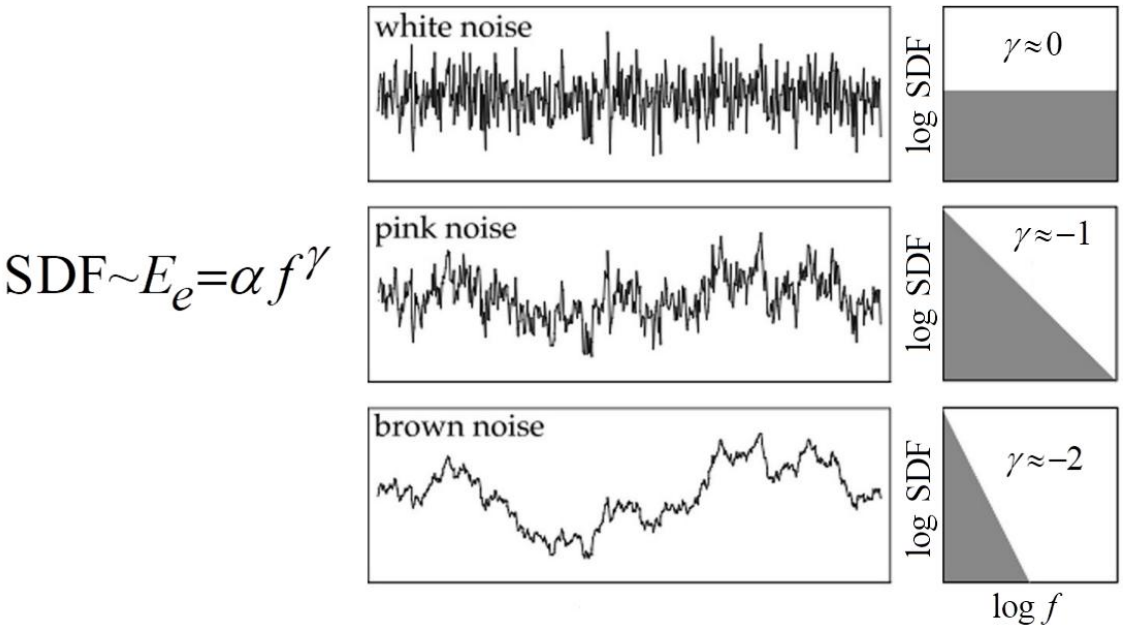

Figure 5. Three typical noises with their associated power spectra (adapted from **[42]**).

(d) Frequency distribution of the events: The frequency distribution during the damage process is originally proposed as an index to be evaluated. In this case, frequencies will be treated in the same way as the amplitudes in the calculation of the *b*-value previously analyzed. Each event will be characterized by a frequency *F* and, in the same way as in the case of the b-value, the signals are characterized by the maximum amplitude.

In the present case, the focus is on finding out if the damage process changes the distribution of the frequencies emitted by the events of acoustic emission. The evolution of this function, represented for the angular coefficient of the statistical

distribution in the bi-log scale called here *c*, is a sensitive precursor of avalanches in the damage regime. Thus, the proposed expression will be:

$$N(\geq F) = \beta F^{-c} \tag{5}$$

where N represents the cumulative number of acoustic emission events with the frequency that characterizes it being at the same time greater than or equal to F, being β and c scalar coefficients. Applying the logarithm in both terms of Eq. (5), we have:

$$logN = \log \beta - c \log F \tag{6}$$

The value c is the slope of the line that links the distribution of events during the damage process as a function of the frequency that characterizes them. The *c*-value, in a similar way that the *b*-value, allows to perceive the changes in the damage process, indicating the imminence of the collapse. If the distribution of these frequencies changes, for example, the number of events with lower characteristic frequencies increases respecting the higher ones, this indicates that a change in the damage process has occurred.

3. PROPOSAL OF AE SIGNAL DETECTION METHODOLOGY

For the analysis of a signal captured by a sensor, defining how to identify the signals of acoustic emission is fundamental. One of the most used techniques known is the technique base on the threshold. In this approach, it is assumed that AE starts when this signal passes the threshold for the first time. Then when it passes below the threshold again, and remains under the threshold for a specific time, the AE signal is said to be completed. In this way, the signal duration in **Figure 2** was determined, Barsoum et al. **[45]**. Moreover, Lu and Chu **[46]** also apply this form to measure the signal duration. However, as noted by Shateri et al. **[23]**, this technique can fail in the presence of signals which are very close among each other, thus, causing considerable errors in the signal counting. In their work, Shateri et al. **[23]** also features the new AE signal detection algorithm by using the root mean square (rms) envelope of AE signal. This function is applied to each AE signal separately. In this way, it is also possible to carry out the identification of the acoustic emission signals manually. However, this method, apart from not being quite precise, may prove to be infeasible when the number of signals to be processed is high.

The following is a semi-automatic proposal for signal identification using MATLAB software **[47]**, which works even when two or more signals are almost coincident. The main advantage of our proposal is to offer an alternative to the systems and

software already available, however, with a relatively simple implementation, maintaining a good precision also when the hits discrimination could be difficult using traditional or most commonly used methodologies. This proposal requires one of the steps to manually review the data, as it can be seen in the following example. The proposed methodology was divided into three main actions: (i) Automatic identification and selection of signals, (ii) manual adjustment, and (iii) analysis of results.

(i) Automatic identification and selection of signals: in this action on the acquired signal (amplitude *vs* time), a threshold value is defined. Next, every peak of positive amplitude is identified. These peaks are classified with indexes 0 (indicated in magenta) or 1 (indicated in black) for values below and above the threshold level, respectively. **Figure 6a** shows, for a typical signal, the position of the threshold level and the identification of indexes 0 and 1 on the signal. Every time there is a change in the index, it means that a signal starts or ends. Within the interval in which a signal starts or ends, the peak of maximum amplitude is identified, disregarding all others. In this way, the duration of the signal and its maximum amplitude is detected. This is illustrated in **Figure 6b**. It is worth noting the importance of defining an appropriate level of threshold. It must be low enough to capture the smaller AE signal. However, it must not be too small in order to allow the correct identification of the starting and ending times of the significant signals.

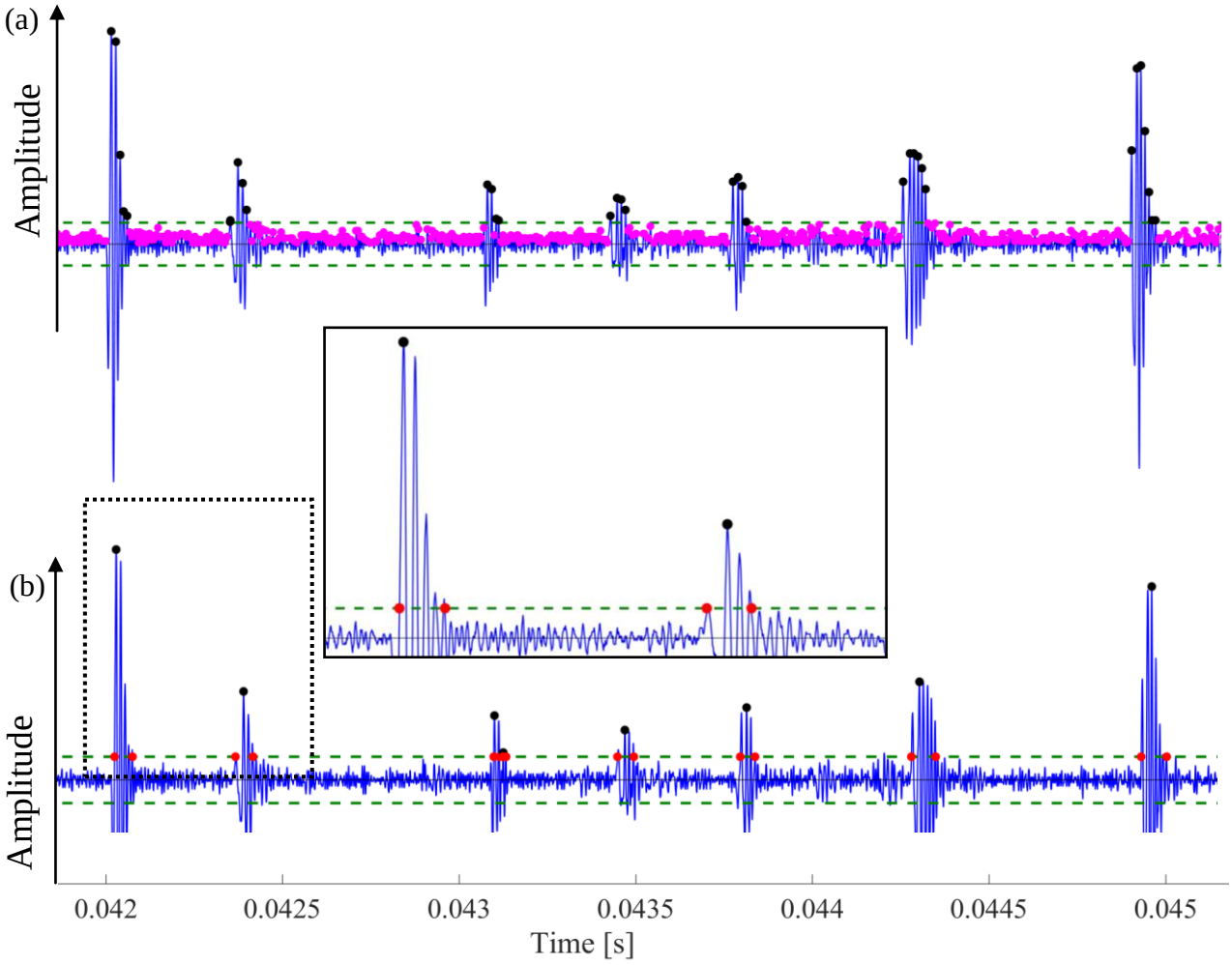

Figure 6. Step representation of the proposed algorithm for detecting acoustic emission signals. (a) AE signal with identification of points below (magenta dots) and above (black dots) the threshold. (b) Signals isolated by the algorithm with identification of the maximum peak (dark blue dots), starting, and ending time (red dots).

(ii) Manual adjustment: In this step, using internal tools from the MATLAB software **[47]**, it is possible to make corrections in some of the automatic determinations performed by the software.

In **Figure 7a**, the determination made by the software is shown, featuring two signals instead one. In the visual adjustment, the user can decide in this case to transform these two signals into one by manually correcting the list of peaks that had been obtained automatically. In this way, the user's criteria modify the automatic determination, defining the situation presented in **Figure 7b**.

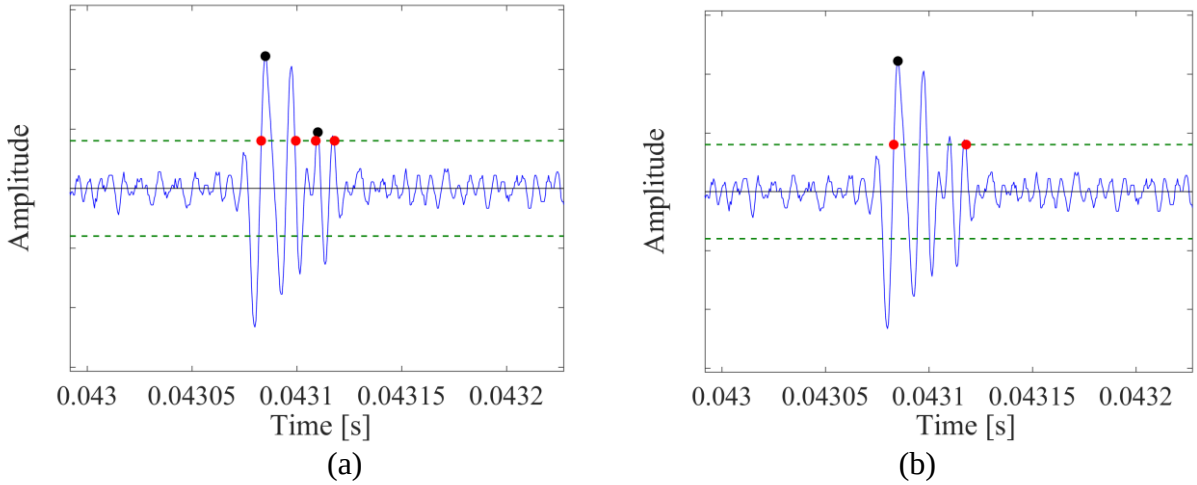

Figure 7. Manual adjustment of automatically determined information: (a) signal identified in the visual inspection for correction, (b) Signal corrected, redefining maximum amplitude peak, start, and end time.

(iii) Analysis of results: In the last step of the procedure, the beginning-end and the maximum amplitude of the signals were already identified. Then, it is possible to calculate other parameters of each signal that will be used in the calculations,

for example, the rise angle (RA), the average frequency (AF), the energy of each event, arrival time, duration, among others.

4. EXPERIMENTAL TEST

The study of acoustic emission was carried out from a glass fiber reinforced polymer (GFRP) specimen. Material similar to that one used by the company "*IMAP Industria e Comércio*" **[48]**, which makes aerial baskets with spears for working at great heights (**Figure 8**).

(a) (b)

Figure 8. (a) Application of the GFRP and (b) detail of the manufacturing of the GFRP rod.

GFRP is a resin compound with a second phase formed by glass fiber, which provides high resistance to traction, flexion, and impact. The resulting mixture is a lightweight, electrically insulating material. There are several ways to manufacture a GFRP

part; the method adopted depends on the application of the component, production volume, surface quality, among other factors. Manual lamination can be carried out, or continuous lamination and details about processing can be found in the literature **[49]**. A manual lamination process was used to perform the specimen tested with fibers randomly arranged in the matrix. Noticed that some parts of the components were built with glass fiber distributed in preferential direction as indicated in **Figure 8b**. The mechanical properties of the tested material are shown in **Table 1**. The density calculation was made from the mass and volume measurement calculated by the geometry of the 2 mm thick sample (see **Figure 9a**).

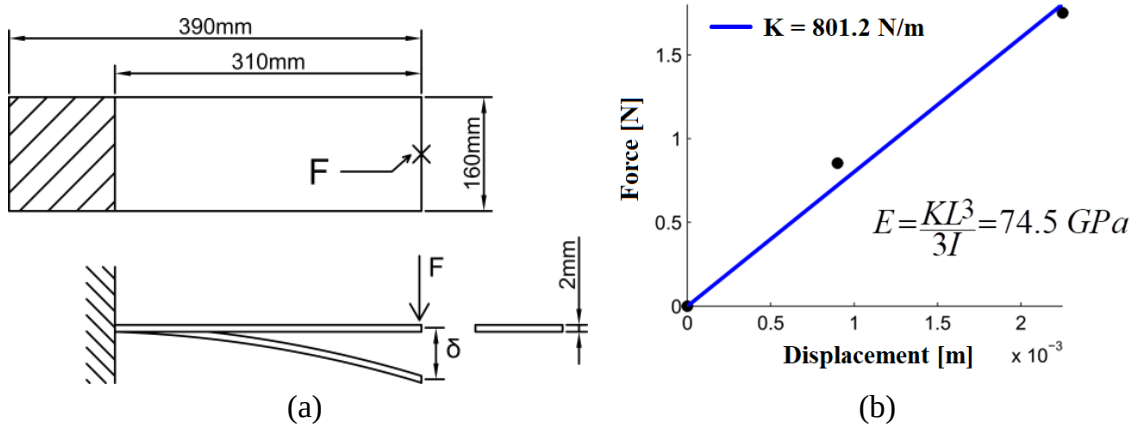

Figure 9. Sample tested to obtain the mechanical properties of the material, a) geometry and layout of the cantilever beam and b) stiffness and elasticity modulus of the material.

The modulus of elasticity is determined by performing a bending test over a cantilever beam made with the composite specimen, as illustrated in **Figure 9a**. Through the force *vs* displacement ratio, the material stiffness (K=801.2 N/m) is obtained and finally the modulus of elasticity is determined (**Figure 9b**), where I is the moment of inertia (I=1.067x10^{-10} m^4).

Table 1. Mechanical properties of the material.

PROPERTY		
Young's modulus	E	74.5 GPa
Mass density	ρ	1450.3 kg/m^3

The test carried out until the rupture be produced to study the damage process of this type of material was performed through the instrumentation of acoustic emission sensors. For this purpose, a sample of the material was subjected to a three-point bending test by using the universal testing machine Emic DL-2000 **[50]**. The sample was tested under deformation control at a speed of 0.1 mm/s. As shown in **Figure 10**, a piezoelectric sensor PCB model 352A60 **[51]** with response frequencies between 5Hz and 60 kHz was used to capture the signals of the elastic waves. The acquisition system was performed using the Pulse software **[52]** with a sampling frequency of 65 kHz. As indicated in Baker **[53]** for the Nyquist theorem to avoid the aliasing problems, the frequency of acquisition must be at least two times the range frequency of interest. In the analyses contained in this work, we

consider a reliable frequency of up to 20 kHz, therefore, having a ratio of 3 times in relation to the acquisition frequency, thus, guaranteeing acceptable control for the aliasing problem. Furthermore, a care was taken during the test to avoid external noise contaminating the test.

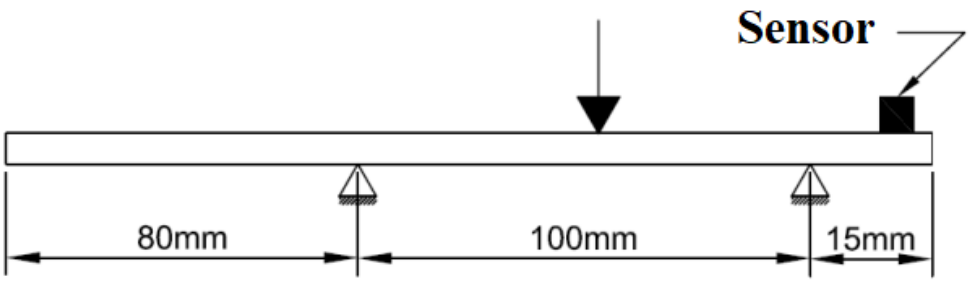

Figure 10. Sample dimensions and conditions of the bending test. Width equal to 40 mm and 2 mm of thickness.

Figure 11 shows the equipment used in the test and the initial and rupture configurations of the tested specimen. The detail in **Figure 11b** shows the fracture region of the plate.

In Elanchezhian et al. **[54]** composites reinforced with glass fibers similar to the ones used in the present work are analyzed. In the study cited in the present work, the Scanning Electron Microscope (SEM) to study the fractured region was used as presented in **Figure 12**.

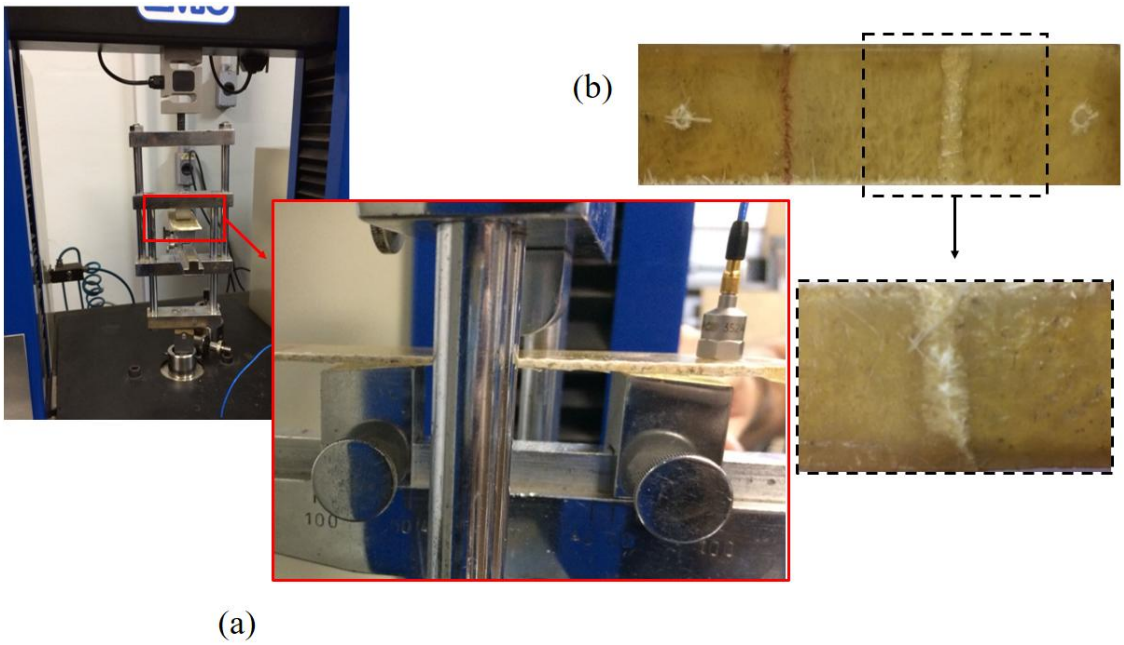

Figure 11. (a) General view of the test machine and detail of the specimen instrumented; (b) Final configuration of the rupture specimen and detail of the fracture.

In this analysis, it was possible to detect the intra fiber delamination as a predominantly mechanism of failure. Furthermore, as expected, the image shows an apparent interfacial adhesion between the matrix and the fiber. The presence of voids depends on the amount of care in the manufacturing of the part, but it is common to observe them when the process is carried out manually as it could be observed in the specimen used in the present work. The random orientation of the glass fibers, as seen in the SEM image in **Figure 12**, allows us to consider isotropic the mechanical behavior of the plate.

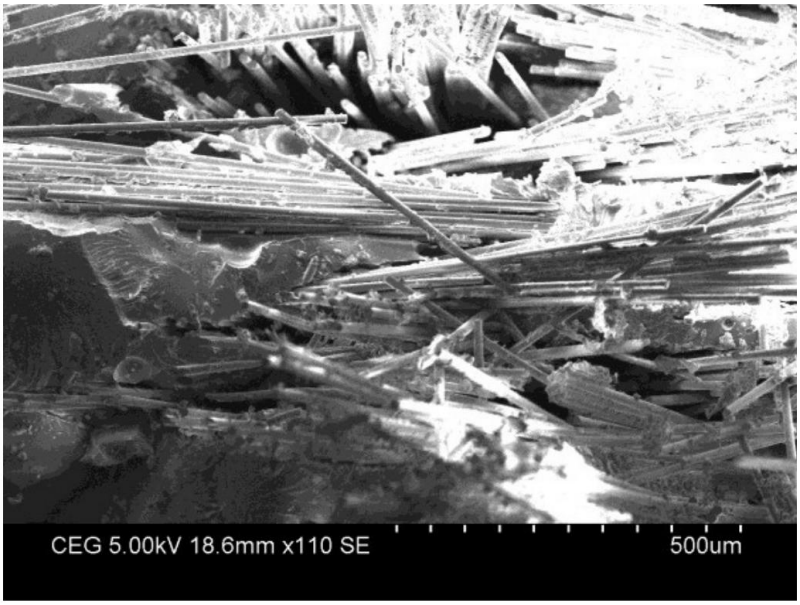

Figure 12. SEM image of GFRP after flexural testing **[54].**

5. RESULTS AND DISCUSSION

5.1 AE signal analysis in time-frequency domain

Figure 13 shows the load versus the time curve as well as the positive part of the acoustic emission signal captured by the sensor. Moreover, the amplitudes of the AE signals *vs* the time, over which the signals take place, are presented. A 6 kHz high pass filter was used to remove the oscillations related to the first four natural frequencies (w_n) of vibration in flexural mode (ω_{n1}=237 Hz, ω_{n2}=1169 Hz, ω_{n3}=1967 Hz and ω_{n4}=3638 Hz). The goal to cut off this frequency is to avoid to contaminate with the natural frequencies the signal frequency content related to the interaction between the mesostructure and the damage produced during the test. From the filtered signal, the methodology

presented in section 3 of this work was applied. The proposed algorithm separated and distinguished approximately 5000 signals. The threshold for detecting the signal was set at 0.25 mV. It is worth mentioning that the output data generated by the Pulse software **[52]** is given in terms of acceleration. However, it is known that there is a linear relationship between acceleration and output voltage.

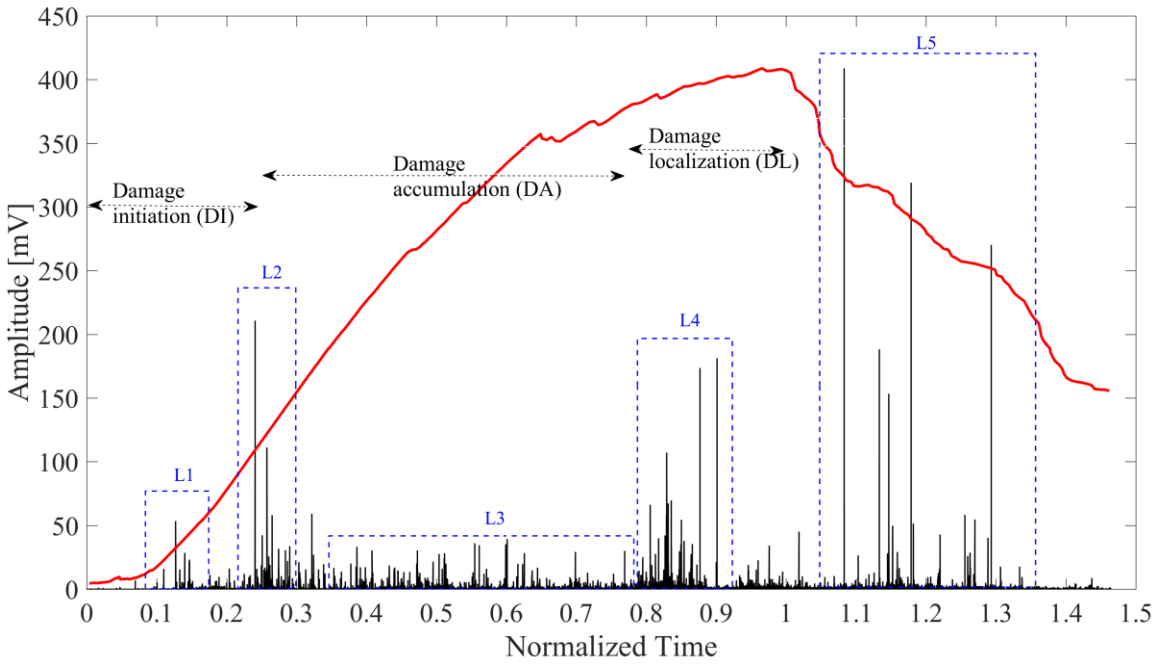

Figure 13. EA test signal and load curve (out of scale). Normalized time in relation to the time in which the maximum peak load occurs at the normalized time = ($time/time_{peak}$).

Notice in **Figure 13** that, at the beginning of the test, two avalanches of events are perceived. The avalanche characterizes a succession of events that are associated. They may indicate that

in some regions of the specimen, there was an abrupt rupture or some other type of disturbance which in turn produces changes located in the energy balance. Among such changes, the dissipated elastic and kinetic energy can be found. The latter being responsible for the emission of elastic waves that reach the sensors placed on the surface of the body and that are registered as acoustic emission signals. The two avalanches illustrated in **Figure 13**, indicated as label L1 and L2, are possibly caused due to the accommodation of the specimen in the supports without significant change in the specimen stiffness.

Subsequently, there is a region of acoustic emission signals with low amplitudes where it is noticed that there is not a significant influence from one event on the other, this region was indicated in **Figure 13** as label L3. Later in the region indicated with Label L4, the new increment in the event avalanches indicates that the regime of the specimen has changed, which can be considered as a precursor of the imminent collapse. Note that there is not great acoustic activity when the maximum load is reached, but the activity restart in the post-rupture process identified by label L5.

The damage process was divided into three intervals. The damage initiation region (DI) [0-0.26s], the region where the damage grows regardless of its sources, called damage accumulation (DA) [0.26-0.78], and the interval where the cracking coalescence takes place (DL) [0.78-1]. In the present analysis, the attention

(in terms of acoustic emission) was concentrated until reaching the maximum load, therefore, the normalized time is given in relation to the maximum peak loading time ($time_{peak}$). These three regions identified changes in the AE signal regime that can be seen both in **Figure 13**, with the description made in the previous paragraph, and in **Figure 14**, where the variation in the number of events during the test is presented. In this last figure, in addition to the number of instantaneous and accumulated events, the evolution of the load and the evolution of the acoustic emission energy during the test are also presented. The energy value was computed using the methodology presented in RILEM **[30]**.

Figure 14 indicates the part of the process that will be analyzed, that is, until reaching the maximum load. After the peak load, there is more recording of the acoustic emission signals as it can be seen in **Figure 13**, but this part of the process will not be analyzed as it was previously mentioned. It could be noted that in **Figure 14** the acoustic emission energy and the number of accumulated events have a considerable correlation. It is possible to identify in the variation of these parameters three slopes that coincide with the three regions previously indicated.

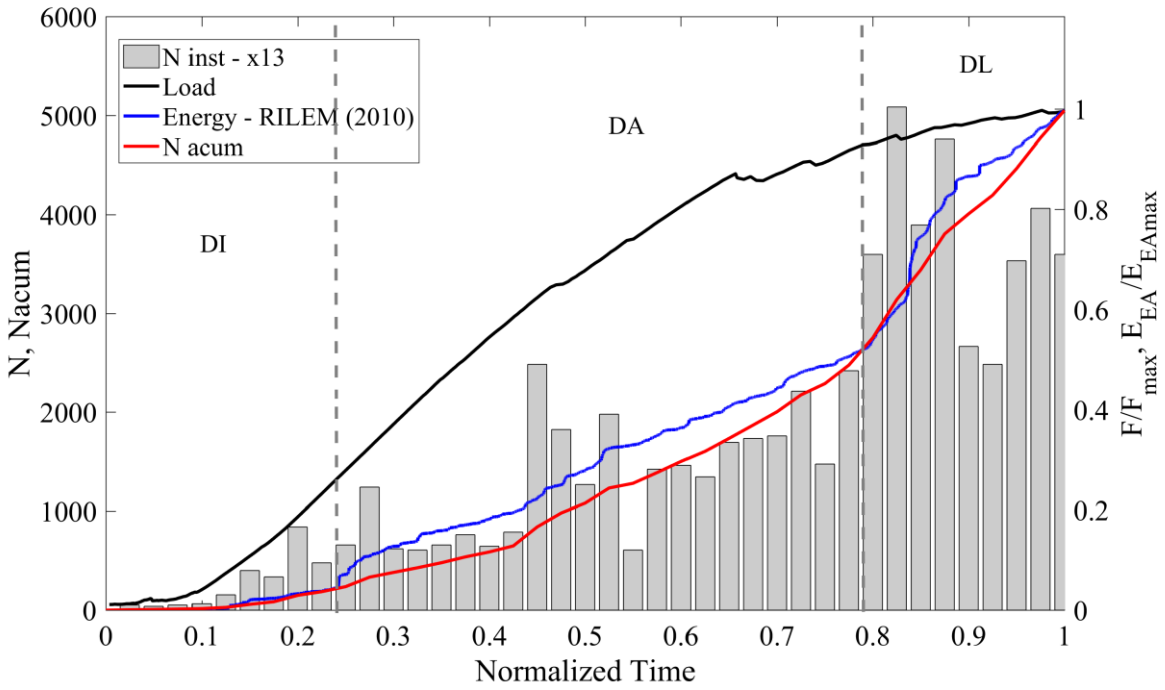

Figure 14. Number of instantaneous events, number of accumulated events and load and accumulated energy versus time. Notice that to maintain the same vertical scale for the instantaneous and accumulated hits, the number of instantaneous hits was multiplied by 13 in the plot.

Figure 15 shows the Fast Fourier Transformed (FFT) of each signal separately and overlapping each one for their analysis in the frequency domain for the three zones previously classified in **Figure 13**. For a better analysis, each zone was divided into four equally spaced time intervals. In these time intervals the FFT frequencies are computed. The load curve and the number of instantaneous events shown in **Figure 14** are still shown out of scale. In the first zone, frequencies between 6 and 12 kHz of low

intensity dominate the analyzed period of time. In the DA zone, the frequencies previously mentioned are highlighted, being able to classify them as typical of material failure mode. Higher frequencies close to 20 kHz appear with less intensity but they can be indicating the emergence of new damage mechanisms. It is important to mention that these high frequencies are close to the Nyquist frequency limit, thus, compromising, partially, the quality of the information in high frequency range.

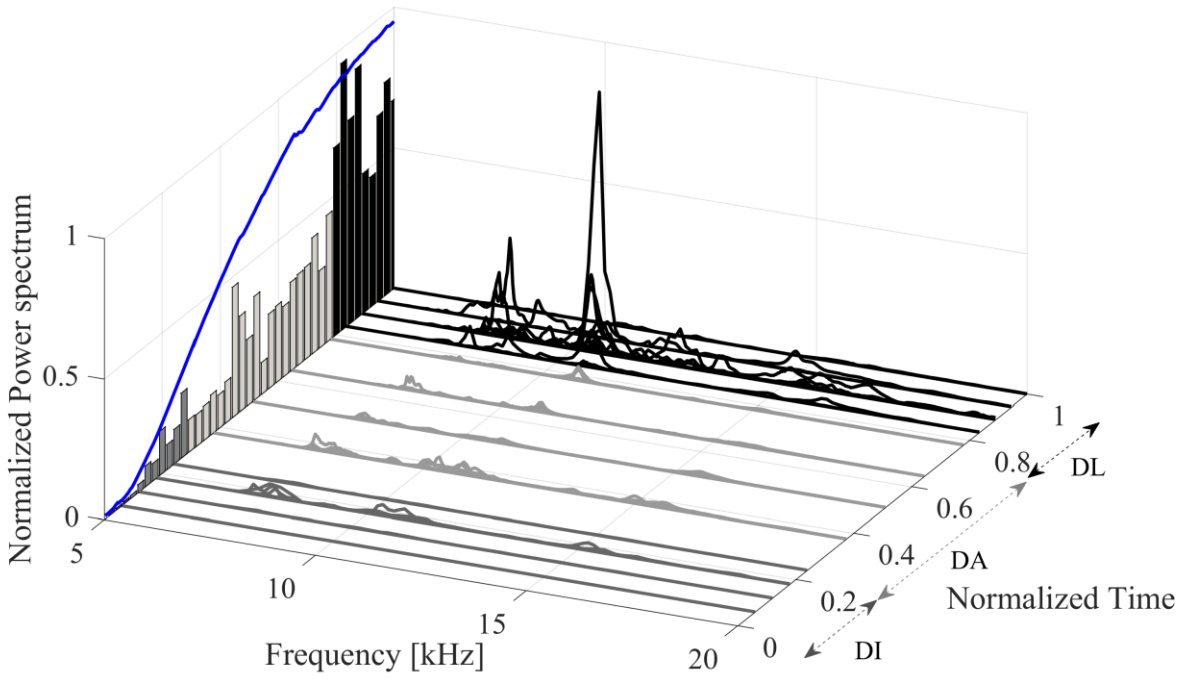

Figure 15. FFT of each signal separately and overlapping, analyzed in the domain of time and frequency in different zones.

Finally, in the DL zone, frequencies of different magnitudes are recorded as they approach the maximum peak load. The transition of the fracture processes changes the excited frequencies. It can be noted that due to the limited response of the employed equipment, the characteristic frequencies associated with real mechanisms linked to the rupture of the reinforced composite, such as delamination, matrix, and fiber breakage, debonding, among others, cannot be established. However, the ability to monitor and predict critical zones is evident by being able to identify a situation of great activity of the acoustic emission events and the subsequent collapse of the structure. Very interesting works could be cited where the link between the signal frequencies content and the failure mechanism is established for the matrix with fibers composite, for example **[55],[56].**

5.2 Fracture mode

The shape of the AE waveforms is reported to be characteristic of the fracture mode (**Figure 3a**) **[17].** The separate or combined rise angle (RA) and the average frequency (AF) parameters are related to the different failure mechanisms as it was already presented in Section 2 of this article. As reported by **[30, 57],** the failure mechanism categorization based on (RA) (AF) produces results less dependent on the type of sensors. **Figure 16** presents the typical characteristic parameters for Modes A and B as well as some examples to exemplify them.

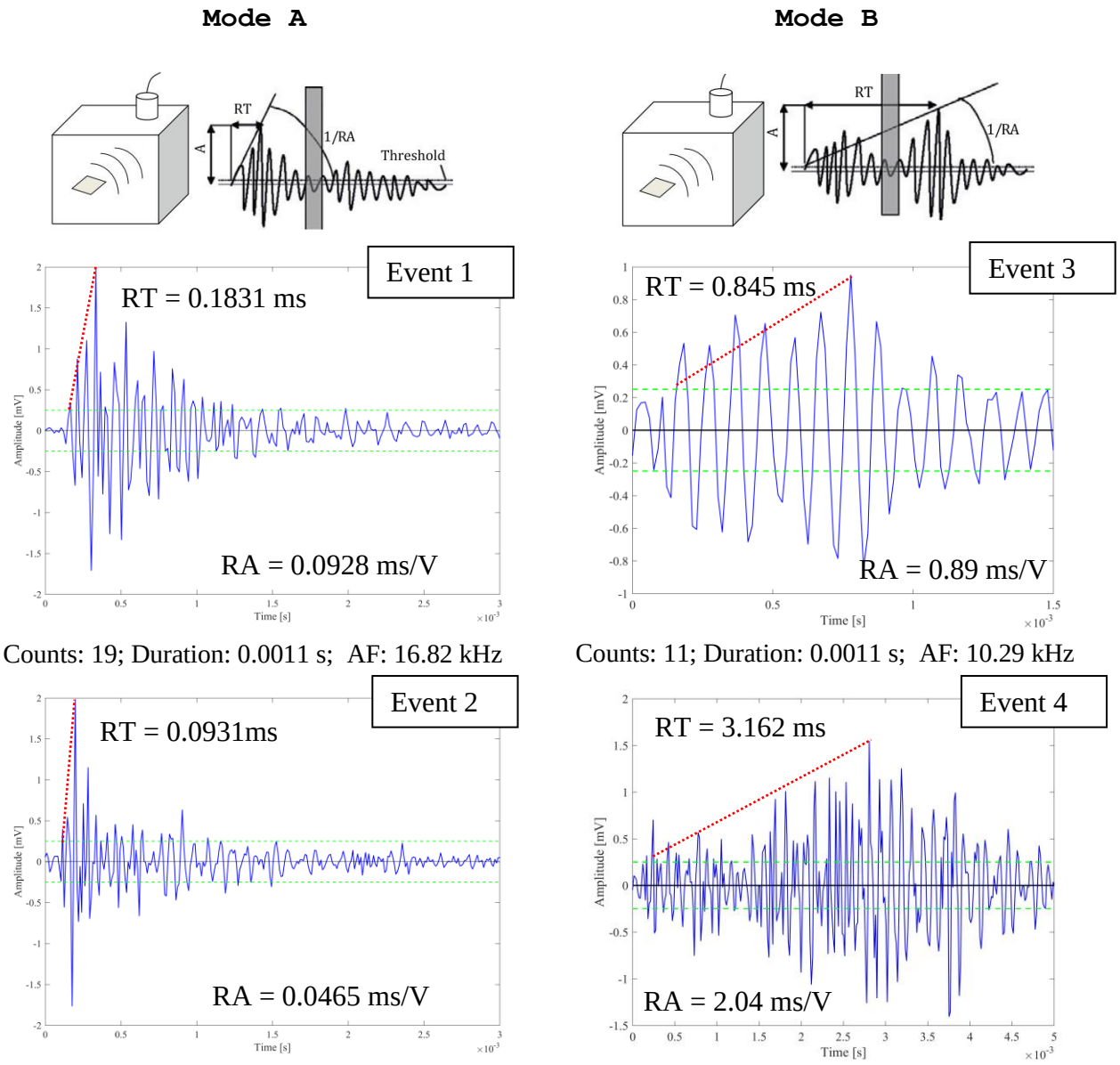

Counts: 19; Duration: 0.0011 s; AF: 16.82 kHz

Counts: 11; Duration: 0.0011 s; AF: 10.29 kHz

Counts: 18; Duration: 0.000974 s; AF: 18.48 kHz

(a)

Counts: 52; Duration: 0.0047 s; AF: 10.99 kHz

(b)

Figure 16. Event classification: a) Mode A and b) Mode B. (Adapted from ref. **[58]**)

It is also possible to notice in **Figure 16a** that there are different waveforms for Mode A, as it has been also observed by Huguet et al. **[11]** when analyzing composites reinforced by tensile

glass fibers as it is shown in **Figure 17**. In Hughet et al. **[11]** work, signals were classified into A-type (Event 1), which has a longer rise time and a slower wave decay, and into B-type (Event 2) that show steep rising and descents. Both are attributed to the damage in the matrix, but they occurred at different stages of the test.

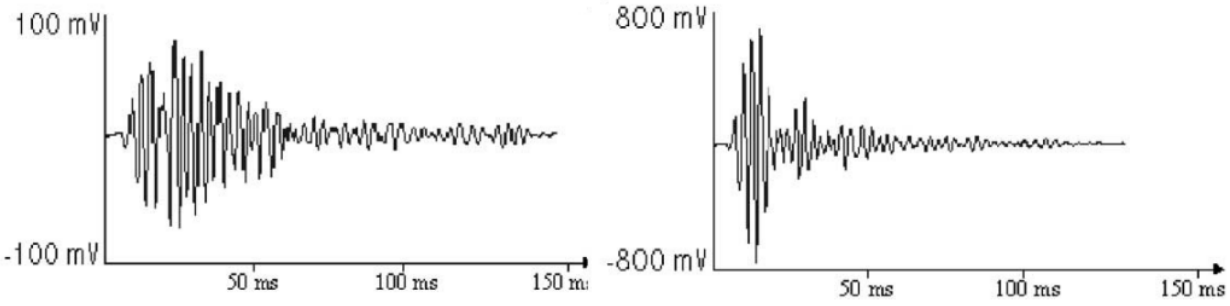

(a) (b)

Figure 17. (a) A-type and (b) B-type waveforms observed by Huguet et al. **[11]** which correspond to different damage mechanisms inside the material.

Based on the events shown in **Figure 16**, a criterion for separating and distinguishing the different events was created. Using the RA/AF ratio, it is possible to identify that Mode A events have a ratio less than 0.006. On the other hand, Mode B events have a ratio greater than 0.055. From the experimental observation and the defined criterion, the division between Modes A (in red) and B (in blue) is shown in **Figure 18**. In this figure, the results in terms of the parameters RA and AF are presented.

The transition region, located between the intervals of A and B, comprises a mix of events that could not be classified as Mode A or B without mischaracterizing other events present in the same zone. Moreover, in **Figure 18** two lines were drawn from the orthogonal diagram origin in order to isolate the events of each mode and the events shown in **Figure 16** are located in the RA AF domain.

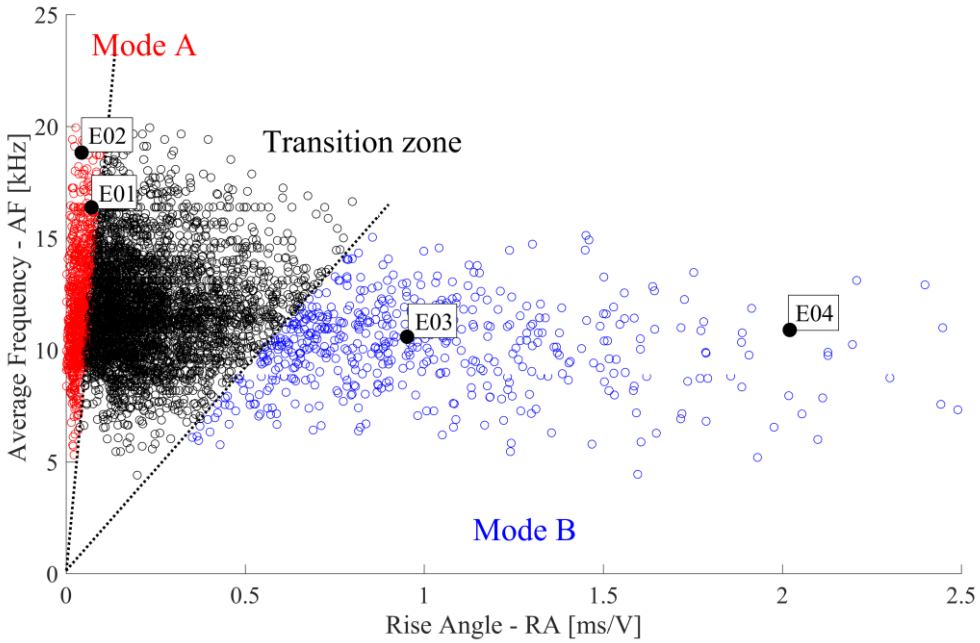

Figure 18. Classification of Fracture Modes based on RA and AF relation and the event localization of the **Figure 16** with E01 (Event 1), E02 (Event 2), E03 (Event 3) and E04 (Event 4).

Figures 19 a-c show a slight transition from Mode A to Mode B throughout the trial.

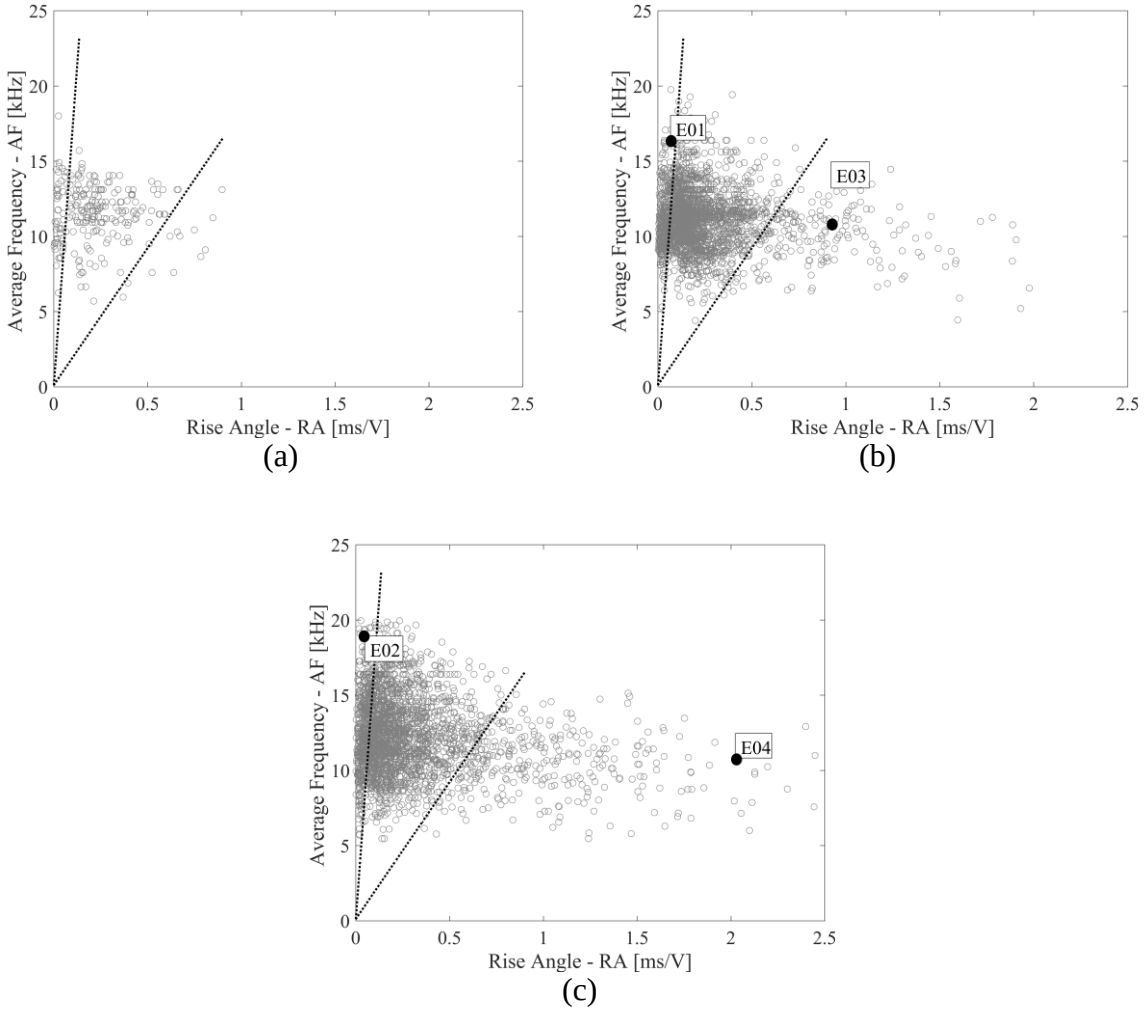

Figure 19. RA and AF relation for different normalized time intervals (a) 0-0.25, (b) 0.25-0.78, and (c) 0.78-1. Normalized time at which events presented in **Figure 16** take place: E01(0.52 s), E02(0.82 s), E03(0.44 s), E04(0.95 s).

Figure 20 shows the evolution of the normalized RA and AF parameters versus the normalized time of the test. The points indicate the value of each event and their colors show the classification according to **Figure 18.** The continuous lines in the

figure represent the moving average computed over 50 values in order to demonstrate the trends of each parameter more clearly.

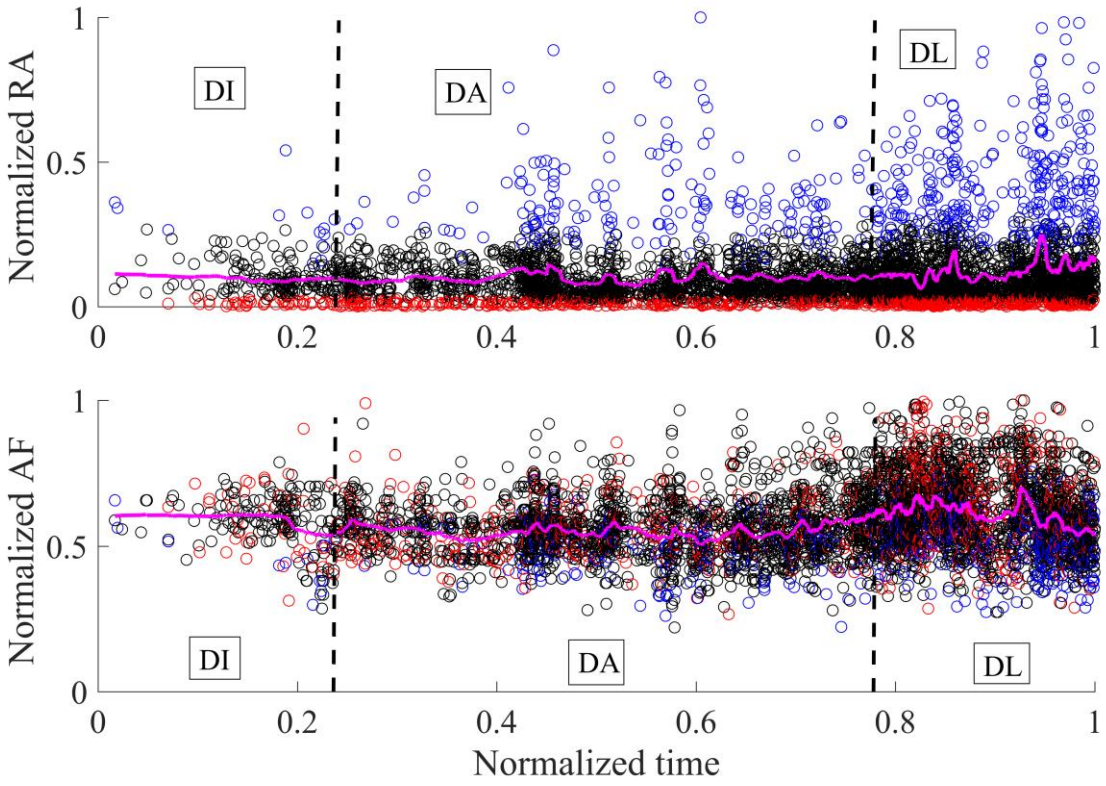

Figure 20. Time history of the RA and AF parameters (points) with the moving average of RA and AF computed over 50 values (continuous line) versus normalized time.

The three zones demarcated in **Figure 13** are also indicated in **Figure 20.** As it can be seen in **Figure 18,** different relations between RA and AF occur simultaneously throughout the test, thus, indicating that Mode A and Mode B events happen in parallel. In addition, in **Figure 20b** it is clearly shown that in the example analyzed it is possible to categorize, grossly speaking, the Modes

of rupture A and B by using only the parameter RA (in ms/V), Mode A (RA > 0.2), transition (0.08 < RA < 0.2)and Mode B (RA < 0.08).

In **Figure 21,** the Coefficient of Variation (CV) of the RA and AF parameters is presented. This coefficient computed as the ratio between the standard deviation and the average values was computed over 50 events indicated as circle dots in the figure. The CV(RA) and CV(AF) variation show a maximum value for the normalize time of 0.58 and also in all the DL region. It should be also noted that the magnitudes of the CV(RA)(around to 100%) was higher than the CV(AF) (around 20%).

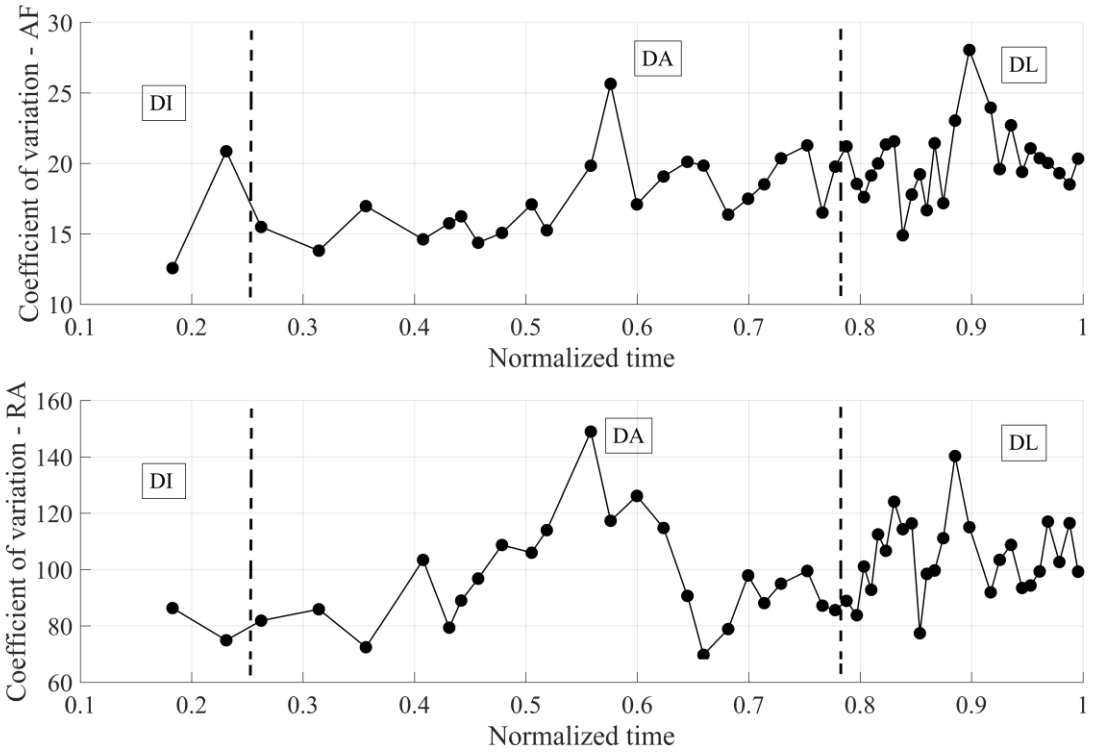

Figure 21. Coefficient of variation in % for AF and RA values *versus* normalized time.

5.3 *b*-Value analysis

Figure 22 shows the *b*-value evolution *vs* time. In the same plot, the load variation and the positive part of the acoustic emission signal captured by the sensor throughout the damage process are also presented. The variation of the parameter *b*-value during the test is shown as being useful when being presented as a precursor of avalanches that can be translated as the nucleation or propagation of a macro crack within the studied specimen. In the present application, the test was divided into 14 intervals, and the *b*-value was calculated in each one of them.

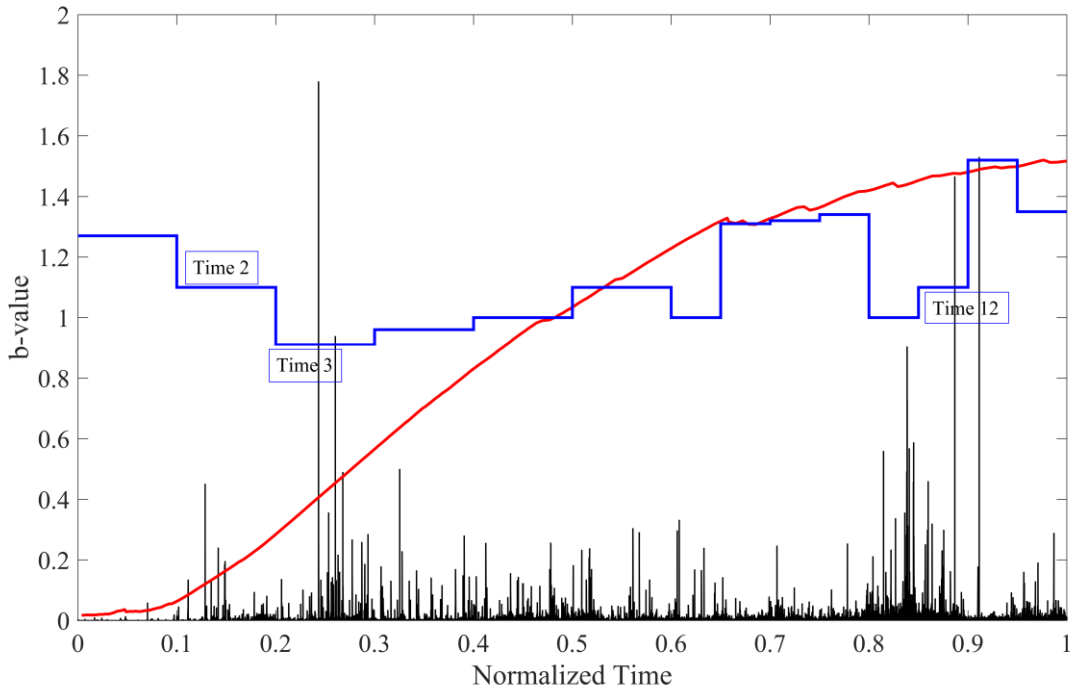

Figure 22. Change in *b*-value during the test. Force and AE signal out of scale.

Figure 23 shows three typical *b*-values obtained during the test and shown in **Figure 22**. **Figure 23d** illustrates the criterion that was followed to identify which points of the graph should be considered to determine the slope that will allow to characterize~~d~~ the b-value. Considering the perfect analogy in statistical terms between AE signals and seismic vibrations generated by earthquakes **[59]** for this criterion the fundamental parameter to be taken into account is the so-called magnitude of completeness, m_c, which applies to both AE signals and earthquakes, i.e. the most frequent magnitude at which 100% of the signals in a space-time volume are detected **[60]**. The correct estimation of m_c is crucial since a value too high leads to the data under-sampling, whereas a value too low leads to a biased analysis. In this study, m_c was calculated according to the maximum curvature method **[61]**. In determining the *b*-value, all events with $m < m_c$ are disregarded and the *b*-value is obtained as the slope of the regression line of Eq. (2). Details on the maximum curvature method and other alternatives for calculating m_c, can be found in the work of Abdel **[62]** where the author shows the application of the technique to the Egyptian National Seismological Network (ENSN) catalogue, and at the same time also observing the relation between m_c and the *b*-value.

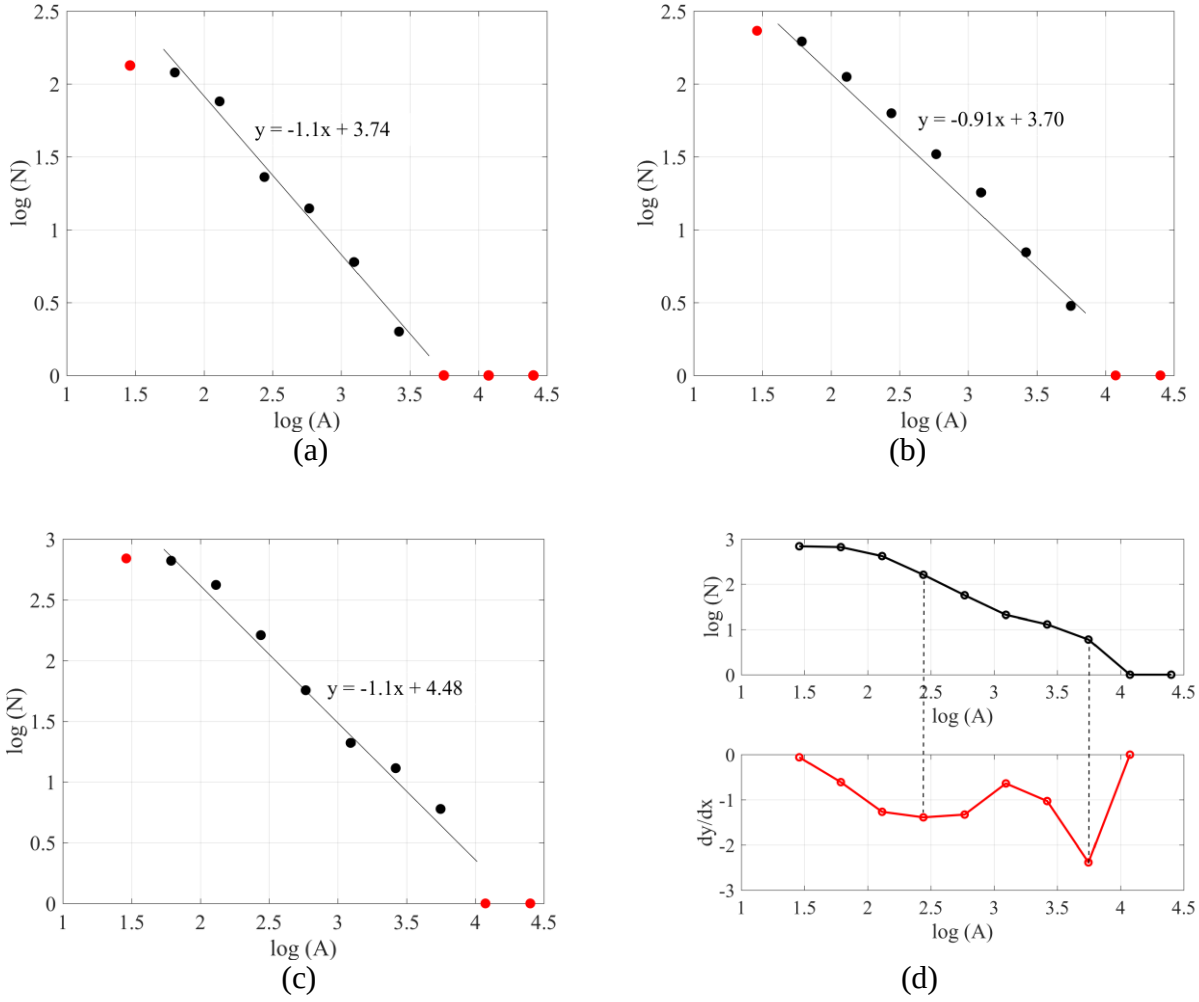

Figure 23. *b*-values obtained at three time intervals during the test, (a) Time 2, (b) Time 3, (c) Time 12 and (d) example of criteria used to determine the b-value.

It is observed that throughout the process in several opportunities, the *b*-value decreases locally when acoustic events of greater amplitude take place. The same trend was noticed in the context of seismology with Cutugno **[63]**, which obtained similar results when analyzing the evolution of the *b*-value in a region of

Aquila, in Italy, over the course of a three-year study. It is interesting to cite here the work of Jung et al. **[64]** that shows the correlation among different failure modes (Matrix cracking, Debonding, and Fiber breakage) their characteristic frequencies and the *b*-value evolution in Carbon fiber reinforced plastic (CFRP) plates. In Birck et al. **[65]**, this phenomenon is also captured by performing the simulation of acoustic emission tests comparing with experimental results, and this phenomenon is discussed.

The values obtained for the *b*-value were within an expected range of [1.5,1.0], but it was not possible to identify the trend shown in **Figure 4** where there is a clear transition from the *b*-value down from values of b = 1.5 to b = 1. This is probably due to the collapse not happening abruptly, that is, there is not a large amount of energy being stored that will have to be released in an explosive collapse. The rupture is happening in a spasmodic form from the DA zone continuing this process in the DL interval.

5.4 Frequency fluctuations

With the aim to obtain frequencies fluctuations of the signal, we have computed the parameter (γ), we used the FFT of each zone classified in **Figure 13**, and then applied the logarithm in both axes, the results are presented at the bottom of below **Figure 24.**

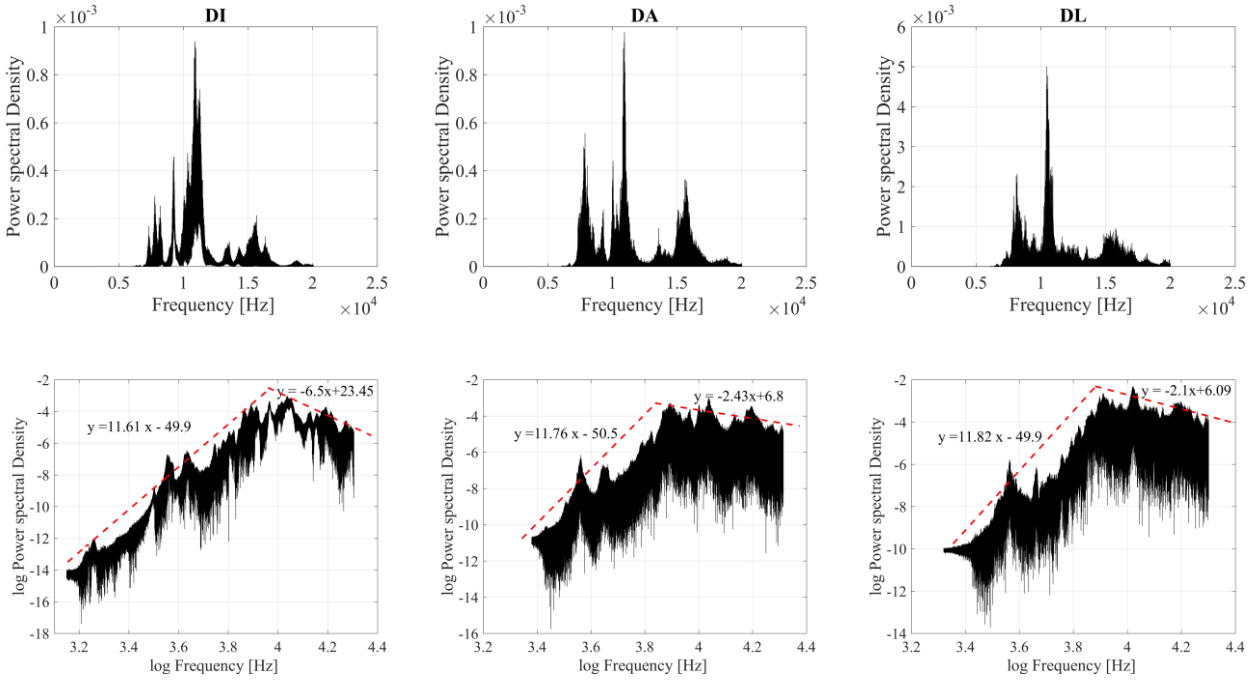

Figure 24. FFT and log-log plot of AE fluctuations in power spectrum density versus the frequency for the specimen test: $1/f$ noise in the (a) damage initiation, (b) damage accumulation and (c) damage localization zone.

It was possible to identify two regions in each graph, the first one in a lower frequency region that did not change its tendency during the test. Whereas, the second region with higher frequency characterizes a brown noise, as it was defined in section 2, shows that the angular coefficient γ falls down from 4 to approximately 2. These results could also be interpreted in accordance with the observation made by Wilson **[66]** that said that when the rupture is imminent an instable phenomenon occurs.

Moreover, then more scale lengths participate in the damage process and the signal has a broad interval of frequency activated. In addition, **Figure 24** is coherent with the results presented in **Figure 15**, where a broad range of frequencies are excited in the third region (DL) when the peak load is imminent.

5.5 Frequency distribution (*c*-Value)

As suggested in item (d) in Section 2 of this work, it is proposed to analyze the distributions of the characteristic frequencies of the events throughout the damage process. The *c*-value parameter seeks to identify variations throughout the test, indicating how the frequency distribution changes during the damage process. The same time intervals used in determining the *b*-value to perform this analysis were used. The weighted average of the frequencies obtained in the FFT, using the spectrum as weight, was considered as a characteristic frequency of the event, an alternative approach to the work of Lacidogna et al. **[44]**. The *c*-value is determined by using the same criteria mentioned in the definition of the *b*-value explained in the previous section and shown in **Figure 23d**. **Figure 25** shows the *c*-values evolution during the damage process. This parameter was computed over 14 intervals.

It could be noted that there is an abrupt change in the *c*-value when it comes close to the local or global rupture. These facts show that the parameter is sensitive when there is a high

activity of events with different frequencies, which makes it a good indicator of imminent failure.

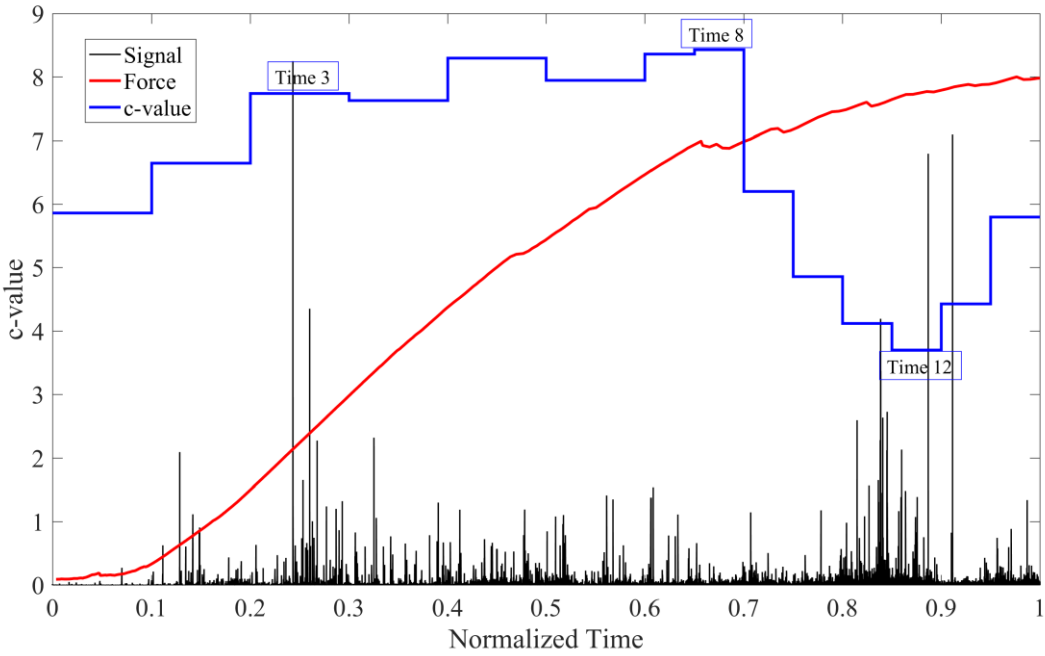

Figure 25. c-values throughout the test (load and AE signal of off-scale).

In **Figure 26** the computation of three *c*-values are presented, and in **Figure 25** the intervals where these specific values were computed are also indicated. When a sequence of successive AE events occurs in short intervals of time, this characterizes an instable phenomenon commonly called avalanche.

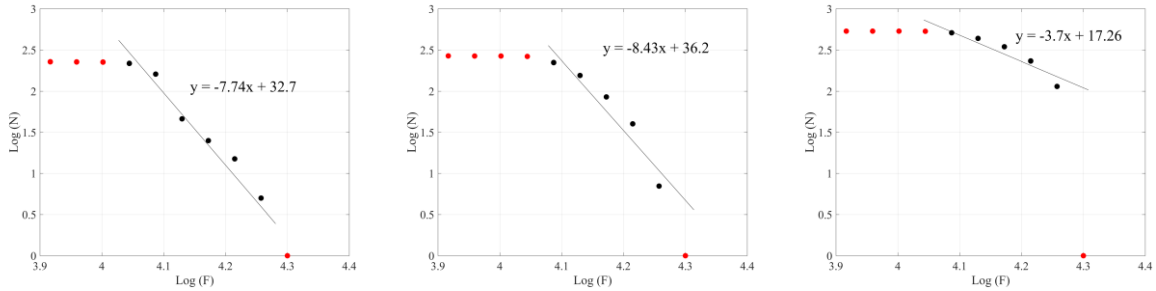

(a) (b) (c)

Figure 26. Calculation of the *c*-values obtained at three time intervals during the test: (a) Time 3, (b) Time 8 e (c) Time 12 are all indicated in **Figure 25.**

At this point, Wilson **[66]** could be cited here, in the sense that in physical instable phenomena, a broad scale lengths are activated. This statement is linked to the decrement in the c-value when the avalanches of events govern the damage process. It can be noticed that when the c-value decrease a wide frequency intervals are activated in the events.

6. CONCLUSION

In the present work, a glass fiber reinforced polymer (GFRP) plate was analyzed using acoustic emission parameters. In addition, the acoustic emission signals are recorded when a plate subjected to a bending test at three points is carried out. AE signals were identified by using a proposed algorithm to perform the signal separation based on defining a specific threshold level. Several global parameters were computed from the signals

acquired. During the course of this study, it was possible to conclude that:

- The algorithm proposed to separate the AE signals allowed to capture them in a semiautomatic way. The results obtained with this system were satisfactory, and it is essential to point out as a good feature of the algorithm the possibility to change eventual automatic wrong signal identification carried out manually.
- The velocity of the number of signals identified during the test, allowed to define three characteristic time intervals: initiate damage (DI), accumulated damage (DA), and localization damage (DL). The amplitudes and frequency range of the signal present a clear pattern in each of these intervals.
- The ratio of the parameters RA and AF obtained during the test correlate with typical signal shapes. The link between this typical signal and the characteristic failure mechanism in the composite material analyzed will be studied in the continuation of our research.
- All the global parameters computed allowed to show different aspects of the evolution of the damage. The *b*-value that measures the signal amplitude distribution decreases when an avalanche traduced by an event with significative magnitude is imminent. The same tendency is expected when the coefficients c and γ also decrease. The

decrease of the *b*-value indicates that more events are produced by the micro fissure coalescence region. More significative avalanches occur in these cases. The decreasing of c and γ indicates that the interval of signal frequency increases. This tendency is coherent with Wilson's **[66]** affirmation since this researcher considers that when a typical unstable phenomenon happens (phase change, chemical reaction, or fracture), more scale length participates in the damage process. Then more frequencies will be excited in the structure when the significative acoustical event is imminent. Notice that the evolution of the c value is an original idea proposed in the present paper and its performance compared with other classical parameters was satisfactory.

ACKNOWLEDGMENTS

The authors wish to acknowledge the CNPq (Brazilian National Council for Scientific and Technological Development) and FAPERGS (Foundation for Research Support of the State of Rio Grande do Sul of Brazil) and the sponsorship guaranteed with basic research funds provided by Politecnico di Torino, Italy for their financial aids in this work.

DATA AVAILABILITY

The raw/processed data required to reproduce these findings cannot be shared at this time due to technical or time limitations.

REFERENCES

[1] ASME-BPVC-Section V. ASME Boiler and Pressure Vessel Code. The American Society of Mechanical Engineers, New York, 2010.

[2] Shiotani T, Fujii K, Aoki T, Amou K. Evaluation of progressive failure using AE sources and improved *b*-value on slope model tests. Prog in Acoust Emiss 1994; 529:534-6.

[3] Kurz JH, Finck F, Grosse CU, Reinhardt H-W. Stress drop and stress redistribution in concrete quantified over time by the *b*-value analysis. Struct Health Monit 2006; 69:81-5.

[4] Carpinteri A, Lacidogna G. Acoustic Emission and critical phenomena: from structural mechanics to geophysics. CRC Press, 2008.

[5] Carpinteri A, Lacidogna G, Corrado M, Di Battista E. Cracking and crackling in concrete-like materials: A dynamic energy balance. Eng Fract Mech 2016; 155: 130-144.

[6] Barile C, Casavola C, Pappalettera G, Vimalathithan PK. Acousto-ultrasonic evaluation of interlaminar strength on CFRP laminates. Compos Struct 2019; 796-805-208.

[7] Djabali A, Toubal L, Zitoune R, Rechak S. An experimental investigation of the mechanical behavior and damage of thick laminated carbon/epoxy composite. Compos Struct 2018; 178:190-184.

[8] Verbruggen S, Aggelis DG, Tysmans T, Wastiels J. Bending of beams externally reinforced with TRC and CFRP monitored by DIC and AE. Compos Struct 2014; 112:113-121.

[9] Ghaib M, Shateri M, Thomson D, et al. Study of FRP bars under tension using acoustic emission detection technique. J Civil Struct Health Monit 2018; 8:285.

[10] Ramirez-Jimenez CR, Papadakis N, Reynolds N, Gan TH, Purnell P, Pharaoh M. Identification of failure modes in glass/polypropylene composites by means of the primary frequency content of the acoustic emission signal. Compos Sci Technol 2004; 1819:1827-64.

[11] Huguet S, Godin N, Gaertner R, Salmon L, Villard D. Use of acoustic emission to identify damage modes in glass fibre reinforced polyester. Compos Sci Technol 2002; 1433:1444-62.

[12] Kumar CS, Arumugam V, Sajith S, Dhakal HN, John R. Acoustic emission characterisation of failure modes in hemp/epoxy and glass/epoxy composite laminates. J Nondestruct Eval 2015; 34.

[13] Barre S, Benzaggagh ML. On the use of acoustic emission to investigate damage mechanisms in glass fibre-reinforced polypropylene. Compos Sci Technol 1992;369:376-52(3).

[14] Hamstad M-A, Testing fiber composites with acoustic emission monitoring. J Acoust Emiss 1982;151:64-3.

[15] Valentin D, Bonniau P, Bunsell A. Failure mechanism discrimination in carbon fiber-reinforced epoxy composites. Composites 1983;345:51-14.

[16] Mechraoui S, Laksimi A, Benmedakhene S. Reliability of damage mechanism localization by acoustic emission on glass/epoxy composite material plate. Compos Struct 2012; 1483:1494-94(5).

[17] Zhou W, Zhao W, Zhang Y, Ding Z. Cluster analysis of acoustic emission signals and deformation measurement for delaminated glass fiber epoxy composites. Compos Struct 2018; 195:349-358.

[18] Othsu M. et al. Recommendation of RILEM TC 212-ACD: acoustic emission and related NDE techniques for crack detection and damage evaluation in concrete. Measurement method for acoustic emission signals in concrete. Mater Struct 2010; 43: 1177–1181.

[19] De Sutter S, Verbruggen S, Tysmans T, Aggelis DG. Fracture monitoring of lightweight composite-concrete beams. Compos Struct 2017; 167:11-19.

[20] Ohtsu M. The history and development of acoustic emission in concrete engineering. Mag Concrete Res 1996; 321:330-48(177).

[21] Colombo IS, Main I, Forde M. Assessing damage of reinforced concrete beam using "*b*-value"analysis of acoustic emission signals. J Mater Civil Eng 2003; 280:286-15(3).

[22] Rao M, Lakshmi KP. Analysis of *b*-value and improved *b*-value of acoustic emissions accompanying rock fracture. Curr Sci India 2005; 1577:1582-89(9).

[23] Shateri M, Ghaib M, Svecova D, Thomson D. On acoustic emission for damage detection and failure prediction in fiber reinforced polymer rods using pattern recognition analysis. Smart Mater Struct 2017;285:300-26.

[24] Soulioti D, Barkoula N, Paipetis A, Matikas T, Shiotani T, Aggelis D. Acoustic emission behavior of steel fibre reinforced concrete under bending. Constr Build Mater 2009; 3532:3536-23(12).

[25] Ohno K, Shimozono S, Sawada Y, Ohtsu M. Mechanisms of Diagonal-Shear Failure in Reinforced Concrete Beams analyzed by AE-SiGMA. J Solid Mech Mater Eng 2007; 462:472-2(4).

[26] Aggelis DG. Classification of cracking mode in concrete by acoustic emission parameters. Mech Res Commun 2011; 153:157-38(3).

[27] Elfergani HA, Pullin R, Holford KM. Damage assessment of corrosion in prestressed concrete by acoustic emission. Constr Build Mater 2013; 925:933-40.

[28] Invernizzi S, Lacidogna G, Carpinteri A. Particle-based numerical modeling of AE statistics in disordered materials. Meccanica 2013; 48:211-220.

[29] Grosse CU, Ohtsu M. Acoustic Emission Testing. Springer Berlin Heidelberg; 2008.

[30] RILEM TC. Recommendation of RILEM TC 212-ACD: acoustic emission and related NDE techniques for crack detection and damage evaluation in concrete: Test method for classification of active cracks in concrete structures by acoustic emission. Mater Struct 2010; 1187:1189-43(9).

[31] Anastassopoulos AA, Philippidis TP. Clustering methodology for the evaluation of acoustic emission from composites. J Acoust Emiss 1995; 11:22-13.

[32] Aggelis DG, Barkoula NM, Matikas TE, Paipetis AS. Acoustic emission monitoring of degradation of cross ply laminates. J Acoust Soc Am 2010; 246:251-127(6).

[33] Richter CF. Elementary seismology. San Francisco and London: W.H. Freeman; 1958.

[34] Hemmer PC, Hansen A. The Distribution of Simultaneous Fiber Failures in Fiber Bundles. ASME. J Appl Mech 1992; 909:914-59(4).

[35] Hansen A, Hammer PC, Pradhan S. The Fiber Bundle Model: Modeling Failure in Materials. 1ed. [S.l.]: Wiley-VCH, 2015-234.

[36] Aki K. Scaling law of seismic spectrum. J Geophys Res 1967; 1217:1231-72(4).

[37] Carpinteri A, Lacidogna G, Niccolini G. Fractal analysis of damage detected in concrete structural elements under loading. Chaos Soliton Fract 2009; 2047:2056-42(4).

[38] Carpinteri A, Lacidogna G, Puzzi S. From criticality to final collapse: evolution of the "b-value" from 1.5 to 1.0. Chaos Soliton Fract 2009; 843:853-41(2).

[39] Han Q, Wang L, Xu J, Carpinteri A, Lacidogna G. A robust method to estimate the b-value of the magnitude–frequency distribution of earthquakes. Chaos Soliton Fract 2015; 81:103–110.

[40] Kogan Sh M. Low-frequency current noise with a 1/f spectrum in solids. Sov Phys Uspekhi 1985; 170:195-28(2).

[41] Mandelbrot BB. Fractal: Form, Chance and Dimension. San Francisco: W H Freeman; 1977.

[42] Gilden DL. Cognitive emissions of 1/f noise, Psychol Rev 2001; 33:56-108(1).

[43] Milotti E. 1/f noise: A pedagogical review. arXiv 2002; physics/0204033.

[44] Carpinteri A, Lacidogna G, Accornero F. Fluctuations of 1/f Noise in Damaging Structures Analyzed by Acoustic Emission. Appl Sci 2018.

[45] Barsoum F, Suleman J, Korcak A, Hill E. Acoustic emission monitoring and fatigue life prediction in axially loaded notched steel specimens. J Acoust Emiss 2009; 40:63-27.

[46] Lu X, Chu F. Shaft Crack Identification Based on Vibration and AE Signals. 2nd International Conference on Vibro-Impact Systems (ICoVIS), Sanya, China; 2010, p.115-126.

[47] MATLAB(R2012a). Natick, Massachusetts: The MathWorks Inc.; 2012.

[48] Imap. https://imap.com.br (Accessed March 20, 2020).

[49] Akovali G, Handbook of Composite Fabrication. Rapra Technology LTDA; 2001.

[50] EMIC - Testing Machines. DL series manual: 500/1000/2000/3000, 3rd edition, São José dos Pinhais-PR. January 2003.

[51] PCB Products. http://www.pcb.com/Products.aspx?m=352A60. (Accessed March 20, 2020).

[52] Brüel & Kjær, Products. http://www.bksv.com. (Accessed March 20, 2020).

[53] Baker M. Demystifying Mixed Signal Test Methods: Chapter 5 - Frequency domain testing and the fft, Newnes, 2003; 115-146.

[54] Elanchezhian C, Vijaya Ramnath B, Hemalatha J. Mechanical Behaviour of Glass and Carbon Fibre Reinforced Composites at Varying Strain Rates and Temperatures, Proc Mat Sci 2014; 1405:1418-6.

[55] Gutkin R, Green CJ, Vangrattanachai S, Pinho S T, Robinson P, Curtis P T. On acoustic emission for failure investigation in CFRP: Pattern recognition and peak frequency analyses. Mech Syst Signal Pr 2011; 25:1293-1407(4)

[56] Barile C, Casavola C, Pappalettera G, Vimalathitan P K. Application of different acoustic emission descriptors in damage assessment of fiber reinforced plastics: A comprehensive review. Eng Fract Mech 2020; 235: 107083.

[57] Ohtsu M, Tomoda Y. Phenomenological model of corrosion process in reinforced concrete identified by acoustic emission. ACI Mater J 2007; 194:200-105(2).

[58] Aggelis DG, Mpalaskas AC, Ntalakas D, Matikas TE. Effect of wave distortion on acoustic emission characterization of cementitious materials. Constr Build Mater 2012; 35:183-190.

[59] Iturrioz I, Lacidogna G, Carpinteri A. Acoustic emission detection in concrete specimens: Experimental analysis and lattice model simulations. Int J Damage Mech 2014; 23: 327-358.

[60] Rydelek PA, Sacks IS. Testing the completeness of earthquake catalogs and the hypothesis of self-similarity. Nature 1989; 337: 251–253.

[61] Wiemer S, Wyss M. Minimum magnitude of complete reporting in earthquake catalogs: Examples from Alaska, the Western United States, and Japan. B Seismol Soc Am 2000; 90: 859-869.

[62] Abdel H. H.E. Estimating the magnitude of completeness for assessing the quality of earthquake catalogue of the ENSN, Egypt. Arab J Geosci 2015; 8: 9315–9323.

[63] Cutugno P. Space-time correlation of earthquakes and acoustic emission monitoring of historical constructions. Doctoral thesis. Polito, Torino, 2016.

[64] Jung D, Mizutani Y, Tdoroki A, Suzuki Y. Change in *b*-Value by AE Propagation Length in CFRP. J Acoust Emiss 2016; 123:129-33.

[65] Birck G, Iturrioz I, Lacidogna G, Carpinteri A. Damage process in heterogeneous materials analyzed by a lattice model simulation. Eng Fail Anal 2016; 157:176-70.

[66] Wilson KG. Problems in Physics with Many Scales of Length. Sci Am 1979; 241:140-157.